# One-step implementation of Rydberg nonadiabatic noncyclic geometric quantum computation in decoherence-free subspaces

Li-Na Sun,[1] F.-Q. Guo,[1] Zheng Shan,[2] M. Feng,[1,3,4,5] L.-L. Yan,[1,*] and Shi-Lei Su[1,†]

[1]*School of Physics and Microelectronics, Key Laboratory of Materials Physics of Ministry of Education, Zhengzhou University, Zhengzhou 450001, China*

[2]*State Key Laboratory of Mathematical Engineering and Advanced Computing, Zhengzhou 450001, China*

[3]*State Key Laboratory of Magnetic Resonance and Atomic and Molecular Physics, Wuhan Institute of Physics and Mathematics, Innovation Academy of Precision Measurement Science and Technology, Chinese Academy of Sciences, Wuhan 430071, China*

[4]*Department of Physics, Zhejiang Normal University, Jinhua 321004, China*

[5]*Research Center for Quantum Precision Measurement, Guangzhou Institute of Industry Technology, Guangzhou 511458, China*

(Received 2 March 2022; revised 12 May 2022; accepted 23 May 2022; published 10 June 2022)

Quantum gates constructed by geometric phase are naturally robust to control errors due to the global nature of the geometric evolution path. Therefore, how to cope with the inevitable decoherence errors is worthy of serious attention for geometric quantum computation. Different from conventional nonadiabatic geometric quantum computation (NGQC), which needs the same evolution time for any geometric rotation angle, we have proposed and experimentally demonstrated nonadiabatic noncyclic geometric quantum computation (NNGQC) without the requirement of the cyclic evolution condition, which thus reduces decoherence errors due to shortened evolution time [J. W. Zhang *et al.*, Phys. Rev. Lett. **127**, 030502 (2021)]. In addition, the use of decoherence-free subspaces (DFS) is another effective strategy to protect quantum gates from dephasing error and has been studied in nonadiabatic holonomic quantum computation [G. F. Xu *et al.*, Phys. Rev. Lett. **109**, 170501 (2012)]. Motivated by previous studies, we propose a one-step scheme to implement single-qubit NNGQC operation in DFS constructed by two Rydberg atoms, and then generalize the scheme to the two-logical-qubit case in one step. The numerical results show that our scheme is robust against decoherence in contrast to the NGQC counterparts. The present scheme combines the features of NNGQC and DFS and can further reduce the impact of decoherence on gate infidelity, which may provide an option for the realization of Rydberg-atom-based quantum computation in the future.

DOI: 10.1103/PhysRevA.105.062602

## I. INTRODUCTION

Quantum computation is considered to be superior to classical computation in solving some specific problems, such as factoring large integers [1] and searching unsorted databases [2]. In order to implement quantum computation, a universal set of single- and two-qubit gates with high fidelity and robustness against errors is essential. In addition, compared with the step-by-step implementation scheme, the one-step implementation scheme of quantum gates greatly reduces the complexity of experimental operation and improves the feasibility of experiments. Therefore, the one-step implementation of high-fidelity robust quantum gates has attracted extensive attention.

In view of the progress in the experimental operation of trapping [3–5] and cooling [6], neutral atoms have become a promising platform in the field of quantum information [7,8]. Rydberg atoms, neutral atoms with large principal quantum numbers that are excited to high-lying Rydberg states, have been studied for construction of quantum logic gates [9–14]. Although many two- and multiple-qubit gates based on Rydberg-Rydberg interactions (RRI) have been experimentally realized to date [3,15,16], the realization of high-fidelity robust quantum gates still faces the challenge of decoherence due to the inevitable interactions between the system and its environment.

Quantum gates constructed based on geometric phases [17–20] depend only on evolutionary paths while being independent of evolutionary details, which is a promising strategy for fault-tolerant quantum computation. However, the originally proposed adiabatic geometric quantum computation [21–23] based on Abelian [18] and non-Abelian [17] phases requires a long evolution time to meet the adiabatic condition, which will amplify the decoherence and reduce the execution efficiency. In order to overcome the limitation of adiabatic conditions, nonadiabatic geometric quantum computation (NGQC) and nonadiabatic holonomic quantum computation based on Abelian [24,25] and non-Abelian [26–31] phases are proposed and experimentally implemented in different quantum systems such as superconducting [25,32–36], nitrogen-vacancy centers in diamond [37–39], and nuclear magnetic resonance [40–44]. In recent years, with the continuous development of NGQC, different optimization schemes of NGQC [45–47] have been proposed. However, both traditional NGQC and time optimized NGQC meet the cyclic evolution condition, which makes NGQC sensitive to decoherence

*llyan@zzu.edu.cn
†slsu@zzu.edu.cn

 

due to the long fixed evolution time limited by the cyclic condition. To overcome the constraints on gate time imposed by cyclic evolution conditions, Refs. [48,49] proposed nonadiabatic noncyclic geometric quantum computation (NNGQC), which effectively overcomes the limitation of the cyclic evolution condition on gate time and thus reduces the impact of decoherence on gate fidelity, and the scheme has been experimentally verified [50].

To further reduce decoherence errors, in addition to the above-mentioned reduction of gate time using NNGQC, the use of decoherence-free subspaces (DFS) [51–54] is also an effective way to protect quantum systems from decoherence. Due to the symmetry structure of the coupling between the system and the environment in DFS, the quantum information encoded in DFS obtains a unified dynamics, so as to effectively prevent the collective decoherence of the system. So far, the DFS scheme has also been experimentally verified in different quantum systems [53–55]. Here, if NNGQC could be implemented in one step in DFS, then this would not only greatly reduce the impact of environmental errors on gate fidelity due to its suppression of dephasing and short evolution times, but the one-step implementation also greatly improves experimental feasibility compared to the step-by-step NNGQC-based two-qubit gate implementation scheme in Ref. [49].

Therefore, how to construct a Hamiltonian in the DFS that implements NNGQC in one step becomes the key to this problem. In this paper, we propose to construct a Hamiltonian under DFS for NNGQC in one step in the Rydberg atom. This scheme realizes the general single-qubit gate and nontrivial two-qubit gate based on NNGQC in DFS, so as to reduce the decoherence error caused by the interaction between environment and system in gate fidelity and realize high-fidelity robust quantum gates. It is worth mentioning that our scheme also has the following two advantages: (i) it takes less time to evolve compared to the previous geometric schemes in DFS [22,27,28,56,57] and (ii) the feature of one-step implementation reduces the complexity of the experiment and provides the possibility for experimental implementation compared to the schemes in Refs. [49,57,58]. In addition, we have conducted numerical simulations to verify the performance of our scheme, including fidelity and robustness, by comparing the proposed NNGQC-based gate in DFS with that of the conventional NGQC-based gate in DFS and the conventional dynamical ones in DFS [dynamical quantum computation (DQC)] with the same dephasing error and spontaneous emission. Although we use the Rydberg atom system to verify the feasibility of our scheme, any quantum platform capable of achieving the same form of effective Hamiltonian is feasible, which means the proposed scheme is independent of the particular physical platform and may have the potential for wider application.

## II. UNIVERSAL SINGLE-QUBIT GATES

We now propose to construct a set of universal NNGQC-based single-qubit gates in DFS. The basic model we study is illustrated in Fig. 1. There is an off-resonant transition between $|r\rangle_i$ and $|g\rangle_i$ with red detuning $\Delta_i$ driven by a classical field of Rabi frequency $\Omega_i e^{i\varphi_i}$. In the interaction picture, it is

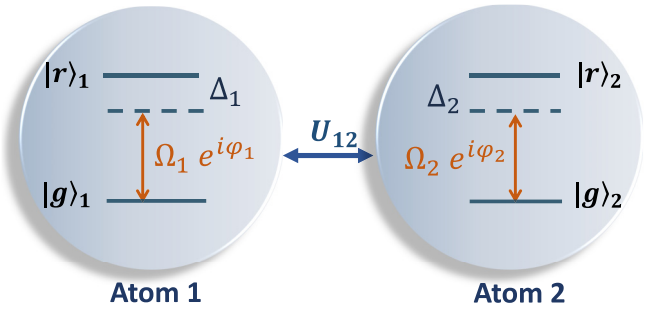


FIG. 1. The diagrammatic sketch of two interacting Rydberg atoms. In $^{87}$Rb atom $i$ ($i = 1,\ 2$), the ground state $|g\rangle_i$ is excited to the Rydberg state $|r\rangle_i$ by an off-resonant laser with Rabi frequency $\Omega_i e^{i\varphi_i}$, and $\Delta_i$ denotes the red detuning between the energy splitting and the driving frequency $\Omega_i e^{i\varphi_i}$. $U_{12}$ is the van der Waals interaction between atoms in the Rydberg state. The distance between atoms is $d_{12} = 7.12\ \mu$m.

modeled by the Hamiltonian (let $\hbar = 1$)

$$H_{\rm I} = \sum_{i=1,2} \frac{\Omega_i}{2} e^{i\varphi_i}(|r\rangle_i\langle g| + {\rm H.c.}) + \sum_{i=1,2} \Delta_i |r\rangle_i\langle r| + U_{12}|rr\rangle_{ij}\langle rr| \quad (1)$$

where $U_{ij}$ denotes the RRI strength between the $i$th atom and the $j$th atom and is denoted as $U_{ij} = \frac{C_6}{d_{ij}^6}$ [59] ($C_6 = 1.043 \times 10^5$ GHz $\mu$m$^6$ is the van der Waals interaction coefficient and $d_{ij}$ represents the distance between the $i$th atom and the $j$th atom). In the limit of large detuning with $\Delta_i \gg \Omega_i$, the Hamiltonian in Eq. (1) satisfies the conditions as $\Delta_1 = \Delta_2 = \Delta$. Using effective Hamiltonian theory, in subspace $\{|rg\rangle, |gr\rangle\}$ the Hamiltonian is rewritten as

$$H_{\rm eff} = \left(\frac{\Omega_1^*\Omega_2}{4\Delta} - \frac{\Omega_1^*\Omega_2}{4(\Delta + U_{12})}\right) e^{i(\varphi_2-\varphi_1)}|gr\rangle\langle rg| + {\rm H.c.} \quad (2)$$

In order to protect the quantum gates from decoherence, we utilize two physical qubits to encode a logical qubit [60,61]. The specific encoding is

$$|0\rangle = |gr\rangle, \quad |1\rangle = |rg\rangle. \quad (3)$$

Therefore, the above effective Hamiltonian in Eq. (2) can be rewritten as

$$H_{\rm eff} = \begin{pmatrix} 0 & \Omega_{\rm eff} e^{-i\varphi} \\ \Omega_{\rm eff} e^{i\varphi} & 0 \end{pmatrix}, \quad (4)$$

in the basis $\{|0\rangle, |1\rangle\}$ with $\Omega_{\rm eff} = \frac{\Omega_1^*\Omega_2}{4\Delta} - \frac{\Omega_1^*\Omega_2}{4(\Delta+U_{12})}$ and $\varphi = \varphi_1 - \varphi_2$. We consider a quantum system described by a time-dependent two-dimensional state subspace spanned by a complete set of orthonormal basis vectors $\{|\psi_k(t)\rangle\}_{k=1}^2$, which following the time-dependent Schrödinger equation $i\frac{d}{dt}|\psi_k(t)\rangle = H_{\rm eff}(t)|\psi_k(t)\rangle$ and the time evolution operator can be described as $U(t,0) = \boldsymbol{T} e^{-i\int_0^t H_{\rm eff}(t')dt'} = \sum_{k=1}^2 |\psi_k(t)\rangle\langle\psi_k(0)|$, $\boldsymbol{T}$ being time ordering. Here we choose a different set of

time-dependent auxiliary states

$$|\mu_1(t)\rangle = \cos\frac{\theta(t)}{2}e^{-i\frac{\lambda(t)}{2}}|0\rangle + \sin\frac{\theta(t)}{2}e^{i\frac{\lambda(t)}{2}}|1\rangle,$$
$$|\mu_2(t)\rangle = \sin\frac{\theta(t)}{2}e^{-i\frac{\lambda(t)}{2}}|0\rangle - \cos\frac{\theta(t)}{2}e^{i\frac{\lambda(t)}{2}}|1\rangle, \quad (5)$$

which satisfies the boundary condition $|\mu_k(0)\rangle = |\psi_k(0)\rangle$ at time $t = 0$. Thus, we can rewrite the state $|\psi_k(t)\rangle = \sum_l C_{lk}(t)|\mu_l(t)\rangle$ and time evolution operator $U(t,0) = \sum_{l,k} C_{lk}|\mu_l(t)\rangle\langle\mu_k(0)|$. Substituting $|\psi_k(t)\rangle = \sum_l C_{lk}(t)|\mu_l(t)\rangle$ into the Schrödinger equation yields $\frac{d}{dt}C_{lk}(t) = i\sum_{l=1}^{L}(\boldsymbol{G}_{kl}(t) - \boldsymbol{D}_{kl}(t))C_{lk}(t)$, where $\boldsymbol{G}_{kl} = \langle\mu_k(t)|i\frac{d}{dt}|\mu_l(t)\rangle$ is the geometric part and $\boldsymbol{D}_{kl} = \langle\mu_k(t)|H_{\rm eff}(t)|\mu_l(t)\rangle$ is the dynamical part. We can obtain the final time ($t = \tau$) evolution operator $U(\tau) = \sum_{l,k=1}^{2}[\boldsymbol{T}e^{i\int_0^\tau(\boldsymbol{G}-\boldsymbol{D})dt}]_{lk}|\mu_l(\tau)\rangle\langle\mu_k(0)|$.

To achieve the noncyclic geometric gates, we choose the auxiliary state $|\mu_k(t)$ satisfying the von Neumann equation [62]: $\frac{d}{dt}\Pi_k(t) = -i[H(t), \Pi_k(t)]$, where $\Pi_k(t) = |\mu_k(t)\rangle\langle\mu_k(t)|$ denotes the projector of the auxiliary basis. Explicitly, the control parameters of the laser can be expressed as

$$\Omega_{\rm eff}(t) = \frac{\dot\theta}{2\sin(\varphi-\lambda)},$$
$$\varphi(t) = \lambda - \arctan\left(\frac{\dot\theta}{\dot\lambda\tan\theta}\right). \quad (6)$$

In this way, we can obtain the time evolution operator as $U(\tau,0) = e^{i\gamma}|\mu_1(\tau)\rangle\langle\mu_1(0)| + e^{-i\gamma}|\mu_2(\tau)\rangle\langle\mu_2(0)|$, in which the global phase $\gamma(\tau) = \int_0^\tau(\boldsymbol{G_{11}} - \boldsymbol{D_{11}})dt = -\int_0^\tau(\boldsymbol{G_{22}} - \boldsymbol{D_{22}})dt = \int_0^\tau\frac{\dot\lambda}{2\cos\theta}dt$ consists of the geometric phase $\gamma_g = \int_0^\tau \boldsymbol{G_{11}}dt = \frac{1}{2}\int_0^\tau\dot\lambda(t)\cos\theta(t)dt$ and the dynamical phase $\gamma_d = \int_0^\tau \boldsymbol{D_{11}}dt = \int_0^\tau\Omega\sin\theta\cos(\varphi-\lambda)dt$, i.e., $\gamma = \gamma_g + \gamma_d$. Since the control parameters of the laser $\{\Omega_{\rm eff}(t), \varphi(t)\}$ all meet the von Neumann equation, the nondiagonal dynamic and geometric phases cancel each other out, i.e., $\boldsymbol{G_{mk}} - \boldsymbol{D_{mk}} = 0$ for $(m \neq k)$ [49]. In order to achieve a purely geometric quantum gate, we set $\varphi - \lambda = \frac{\pi}{2}$ to eliminate the dynamic phase in the evolution process.

Next, we consider that noncyclic geometric quantum computation is different from general NGQC in that it satisfies the cyclic evolution condition, so we use a geodesic line [63,64] to connect the end point of the actual evolution path to the starting point to form path $P_2$, such that path $P_2$ complements the actual evolution path $P_1$ into a closed path $P$. In this way we know that the overall geometric phase is $\gamma_g = \frac{\Omega_{\rm angle}}{2}\int_{\lambda(0)}^{\lambda(\tau)}\int_{\theta(0)}^{\theta(\tau)}\frac{1}{2}\sin\theta d\theta d\lambda$, based on the fact that the overall geometric angle is half of the solid angle $\Omega_{\rm angle}$ enclosed by the closed path $P$ [46].

Then the resulting unitary evolution becomes purely geometric as $U(\tau) = e^{i\gamma_g}|\mu_1(\tau)\rangle\langle\mu_1(0)| + e^{-i\gamma_g}|\mu_2(\tau)\rangle\langle\mu_2(0)|$, which is expressed in the subspace spanned by $\{|0\rangle, |1\rangle\}$ as

$$U = \begin{pmatrix} U_{11} & U_{12} \\ U_{21} & U_{22} \end{pmatrix}, \quad (7)$$

where $U_{11} = e^{-i\frac{\lambda_-}{2}}(\cos\gamma_g\cos\frac{\theta_-}{2} + i\cos\frac{\theta_+}{2}\sin\gamma_g)$, $U_{12} = e^{-i\frac{\lambda_+}{2}}(-\cos\gamma_g\sin\frac{\theta_-}{2} + i\sin\frac{\theta_+}{2}\sin\gamma_g)$, $U_{21} = U_{12}^*$, and $U_{22} = U_{11}^*$ with $\lambda_\pm = \lambda(\tau) \pm \lambda(0)$ and $\theta_\pm = \theta(\tau) \pm \theta(0)$. Therefore, any single-qubit gate can be realized by selecting different $\gamma$, $\lambda_\pm$, and $\theta_\pm$. That is, the initial and final values of auxiliary variables $\lambda$ and $\theta$ are determined by the target geometric gate.

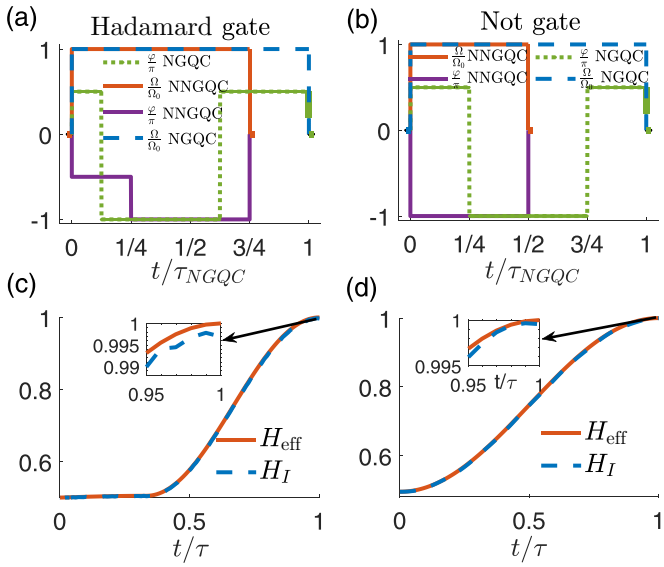


FIG. 2. (a) The Rabi frequency $\Omega_{\rm eff}(t)$ and phase $\varphi(t)$ of the Hadamard gate for NNGQC and NGQC. (b) The Rabi frequency $\Omega_{\rm eff}(t)$ and phase $\varphi(t)$ of the NOT gate for NNGQC and NGQC. Dynamics of gate fidelities of the Hadamard gate (c) and the NOT gate (d) driven by original Hamiltonian $H_{\rm I}$ (orange solid line) and effective Hamiltonian $H_{\rm eff}$ (blue dashed line), respectively. $\Omega_1 = \Omega_2 = 2\pi \times 20$ MHz, $\Delta_1 = \Delta_2 = \Delta = 10\Omega_1 = 2\pi \times 200$ MHz, $U_{12} = \frac{C_6}{d_{12}^6} = 2\pi \times 800$ MHz.

Based on the above discussion of the auxiliary variables $\lambda(t)$ and $\theta(t)$ and the constraints of the pulse parameters $\Omega_{\rm eff}(t)$ and $\varphi(t)$ in Eq. (6) we set the auxiliary variables as

$$\theta(t) = 2\Omega_{\rm eff}t - \theta_0,$$
$$\lambda(t) = \phi\epsilon(t) + \phi_0, \quad (8)$$

where $\epsilon(t)$ is a step function with $\epsilon = 0$ in the first time period $t \in [0, \frac{\theta_0}{2\Omega_{\rm eff}}]$ and $\epsilon = 1$ in the second $t \in [\frac{\theta_0}{2\Omega_{\rm eff}}, \tau]$, and $\frac{\phi}{2}$ denotes the geometric phase $\frac{\phi}{2} = \gamma = \int_0^\tau\frac{1}{2}\dot\lambda\cos\theta dt$ generated by the sudden change during the evolution; $\Omega_{\rm eff}$, $\phi$, $\phi_0$, and $\theta_0$ are constants. With the above settings, we know that the evolution time is $\tau = \frac{\theta_-}{2\Omega_{\rm eff}}$.

We then illustrate the performance of our scheme using a Hadamard gate (achieved by setting $\gamma = \frac{\pi}{4}$, $\theta_+ = \frac{\pi}{2}$, $\theta_- = \frac{3\pi}{2}$, $\lambda_+ = \frac{\pi}{2}$, and $\lambda_- = \frac{\pi}{2}$) and a NOT gate (achieved by setting $\gamma = \frac{\pi}{2}$, $\theta_+ = \pi$, $\theta_- = \pi$, $\lambda_+ = 0$, and $\lambda_- = \pi$) as examples. First of all, according to Eq. (6) and the above discussion about the pulse parameters, the optimized pulse parameters are shown in Figs. 2(a) and 2(b) for the Hadamard gate and NOT gate, respectively. It is clear that compared with the evolution time of the conventional NGQC our scheme takes $\tau_H = \frac{3\pi}{4\Omega_{\rm eff}}$ and $\tau_X = \frac{\pi}{2\Omega_{\rm eff}}$ to construct the Hadamard gate and NOT gate, respectively, which is obviously smaller than the evolution time of the conventional NGQC, and this is the

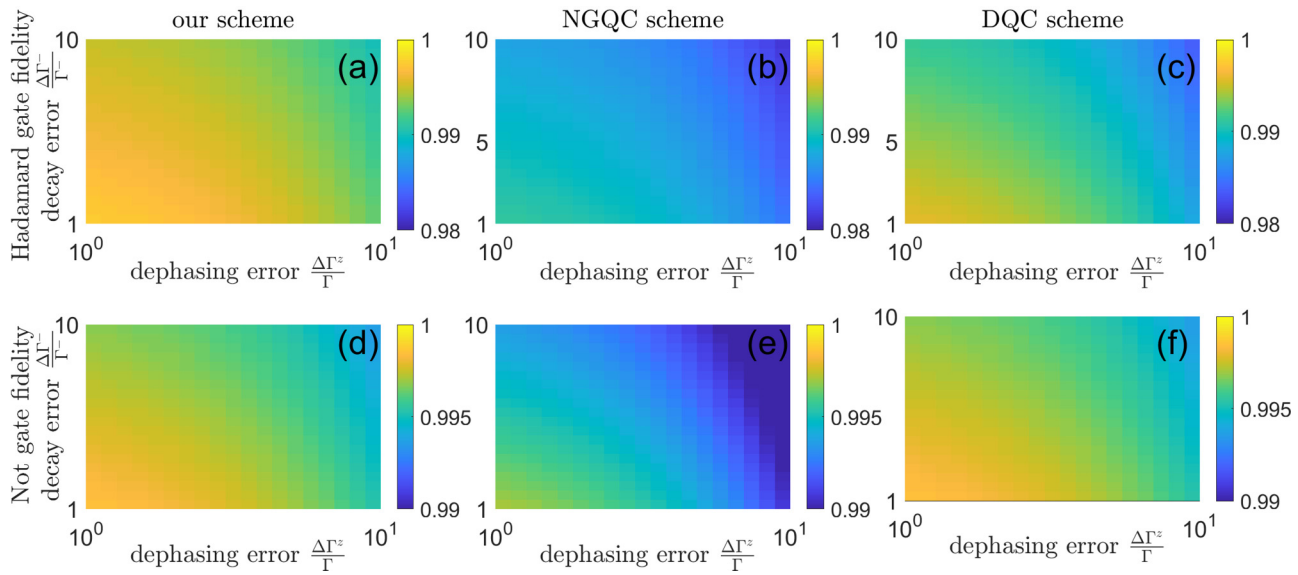


FIG. 3. The Hadamard gate fidelity in the case of NNGQC (a), NGQC (b) and DQC (c) and the NOT gate fidelity in the case of NNGQC (d), NGQC (e), and DQC (f) in DFS under spontaneous emission and dephasing, respectively.

reason why the scheme works well in resisting decoherence, as we will discuss below.

Next, we further illustrate the performance of our scheme through numerical simulations. According to the effective approximation condition $\Delta_i \gg \Omega_i$ of Eq. (2), we set $\Omega_1 = \Omega_2 = 2\pi \times 20$ MHz, $\Delta_1 = \Delta_2 = \Delta = 10\Omega_1 = 2\pi \times 200$ MHz, $U = 2\pi \times 800$ MHz, and the Stark shift term in $H_{\text{eff}}$ is eliminated by further lasering. Then we plot the dynamics of the average fidelities of the gates driven by the original Hamiltonian $H_{\text{I}}$ and the effective Hamiltonian $H_{\text{eff}}$, respectively, in Figs. 2(c) and 2(d). Here, we introduce a concept of average fidelities $F(t) = \frac{1}{2\pi}\int_0^{2\pi} d\alpha \langle\psi_U|U(t)|\psi(0)\rangle$, and the initial states of the system are expressed by $|\psi(0)\rangle = \cos\alpha|0\rangle + \sin\alpha e^{i\beta}|1\rangle$ with $\{\alpha, \beta\} \in [0, 2\pi]$. From Figs. 2(c) and 2(d), we can see that the fidelities of the gates driven by the original Hamilton $H_{\text{I}}$ and the effective Hamilton $H_{\text{eff}}$, respectively, almost fit, and the fidelities of the Hadamard and NOT gates driven by the original Hamilton $H_{\text{I}}$ are divided into 0.9969 and 0.9996, which proves the validity of our original Hamilton $H_{\text{I}}$.

Furthermore, we consider that gate fidelity in open quantum systems is inevitably affected by spontaneous decay and dephasing. Therefore, the dynamic evolution of the system is controlled by the following Lindblad master equation [65]:

$$i\frac{\partial\rho}{\partial t} = -i[H_{\text{I}}, \rho] + \frac{1}{2}\sum_{i\in 1,2}[\Gamma_i^- L(\sigma_i) + \Gamma^z L(\sigma_z)], \qquad (9)$$

in which $\rho$ is the density matrix of the system, $H_{\text{I}}$ is the Hamiltonian of the system in Eq. (1), and $L(\sigma_i) = 2\sigma_i\rho\sigma_i^\dagger - \sigma_i^\dagger\sigma_i\rho - \rho\sigma_i^\dagger\sigma_i$. Also, $\sigma^i = |g\rangle_i\langle r|$ $(i = 1, 2)$ represents the spontaneous decay from the Rydberg state $|r\rangle_i$ to the ground state $|g\rangle_i$, and $\sigma_z = |g\rangle_i\langle g| - |r\rangle_i\langle r|$ represents dephasing of the system. Here we encode the Rydberg state and the ground state as $|r\rangle \equiv |103S\rangle$ and $|g\rangle \equiv |5S_{1/2}, F = 2, m_F = 0\rangle$, and the transition is a two-photon process. The decay rate from the Rydberg state $|r\rangle_i$ to the ground state $|g\rangle_i$ is $\Gamma_1^- = \Gamma_2^- = \Gamma = 0.75$ KHz (where $\Gamma = \frac{1}{T}$ and $T = 1330.8\,\mu$s denotes the lifetime of the Rydberg state $|r\rangle \equiv |103S\rangle$ at about 0 K [15,66,67]) and the dephasing rate $\Gamma^z \in (\Gamma, 10\Gamma)$.

Next, taking the Hadamard gate [Figs. 3(a)–3(c)] and NOT gate [Figs. 3(d)–3(f)] as examples, we compare the robustness of our scheme with the NGQC scheme [25,68] and DQC scheme [69] (see the Appendix for details) in DFS under environmental errors (spontaneous emission and dephasing). As shown in Fig. 3, our scheme has some advantages under the influence of decoherence error.

## III. NONTRIVIAL TWO-QUBIT GATES

To implement a complete set of gate operations in any circuit model for quantum computation requires at least one nontrivial two-qubit gate in addition to a generic set of single-qubit gates. Next, we will show in the following how to implement a universal two-qubit gate based on NNGQC in DFS in one step, and discuss the performance of this two-qubit scheme. As shown in Fig. 4, the transitions $|g\rangle_3 \leftrightarrow |r\rangle_3$ and $|g\rangle_4 \leftrightarrow |r\rangle_4$ are driven by two pulses of $\Omega_3 e^{i\varphi_3}$ and $\Omega_4 e^{i\varphi_4}$, respectively, with the same red detuning, i.e., $\Delta_3 = \Delta_4 = \Delta$. Note that the RRI is generated when atom 2 is in the excited state $|r\rangle_2$. In the interaction picture, the Hamiltonians can be written as (let $\hbar = 1$)

$$H_{\text{I}} = \sum_{i=3,4}\frac{\Omega_i}{2}e^{i\varphi_i}(|r\rangle_i\langle g| + \text{H.c.}) + \sum_{i=3,4}\Delta_i|r\rangle_i\langle r| + \sum_{i\neq j}U_{ij}|rr\rangle_{ij}\langle rr|, \qquad (10)$$

where $U_{ij}$ contains $U_{23}$, $U_{24}$, and $U_{34}$ when atom 2 is in the excited state. Then we extend the Hamiltonian to the form of the four-atom basis, and under the condition of effective Hamiltonian approximation $\Delta_i \gg \Omega_i$ and $\Delta_3 = \Delta_4 = \Delta$ the

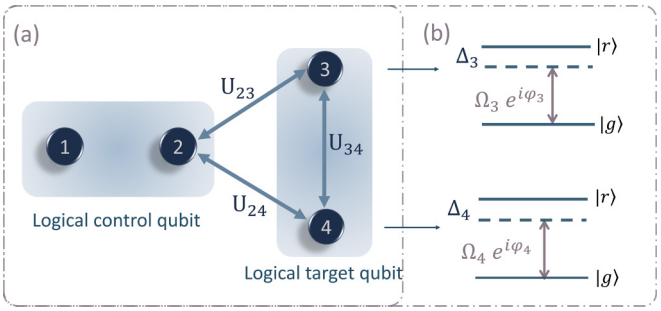


FIG. 4. (a) Four identical Rydberg atoms in a two-dimensional optical lattice. Atom 1 and atom 2 constitute a logic control qubit, and atom 3 and atom 4 constitute a logic target qubit. The distances between atoms 2–4 are the same, i.e., $d_{23} = d_{24} = d_{34} = 3.44\ \mu$m, and therefore they have the same van der Waals forces between them, i.e., $U_{23} = U_{24} = U_{34} = 2\pi \times 10^4$ MHz. (b) Schematic diagram of two identical two-level atoms in atom 3 and atom 4. In atom 3 and atom 4, ground states $|g\rangle_3$ and $|g\rangle_4$ are driven nonresonantly to excited states $|r\rangle_3$ and $|r\rangle_4$ by the classical field of Rabi frequency $\Omega_3 e^{i\varphi_3}$ and $\Omega_4 e^{i\varphi_4}$, with red detuning $\Delta_3$ and $\Delta_4$, respectively. In order to facilitate the analysis and design, we set $\Delta_3 = \Delta_4$, $|\Omega_3| = |\Omega_4|$.

Hamiltonian can be simplified to

$$H_{\text{eff}} = \frac{\Omega_3^*\Omega_4}{4}\mathbf{A}e^{i(\varphi_4-\varphi_3)}|grrg\rangle\langle grgr| + \frac{\Omega_3^*\Omega_4}{4}\mathbf{B}e^{i(\varphi_4-\varphi_3)}|rggr\rangle\langle rgrg| + \text{H.c.}, \quad (11)$$

where $\mathbf{A} = \frac{1}{\Delta+U_{24}} - \frac{1}{\Delta+U_{24}+U_{34}}$ and $\mathbf{B} = \frac{1}{\Delta} - \frac{1}{\Delta+U_{34}}$. We set $U_{23} = U_{24} = U_{34} \gg \Delta$ to further simplify the Hamiltonian in Eq. (11) to obtain

$$H_{\text{eff}} = \frac{\Omega_3^*\Omega_4}{4\Delta}e^{i(\varphi_4-\varphi_3)}|rggr\rangle\langle rgrg| + \text{H.c.} \quad (12)$$

According to Eq. (3) we obtain the effective Hamiltonian in the logical subspace $\{|00\rangle, |01\rangle, |10\rangle, |11\rangle\}$:

$$H'_{\text{eff}} = \begin{pmatrix} 0 & 0 & 0 & 0 \\ 0 & 0 & 0 & 0 \\ 0 & 0 & 0 & \Omega'_{\text{eff}}e^{-i\varphi'} \\ 0 & 0 & \Omega'_{\text{eff}}e^{i\varphi'} & 0 \end{pmatrix}, \quad (13)$$

where $\Omega'_{\text{eff}} = \frac{\Omega_3^*\Omega_4}{4\Delta}$ and $\varphi' = \varphi_3 - \varphi_4$. Since the form of Eq. (13) is similar to that of Eq. (4), we use the same pulse in Eq. (6) to construct one noncyclic geometric quantum operation to obtain the evolution operator of the controlled two-qubit gate

$$U' = \begin{pmatrix} 1 & 0 & 0 & 0 \\ 0 & 1 & 0 & 0 \\ 0 & 0 & U_{11} & U_{12} \\ 0 & 0 & U_{21} & U_{22} \end{pmatrix}, \quad (14)$$

where $U_{11}$, $U_{12}$, $U_{21}$, and $U_{22}$ are the same as the matrix element in Eq. (7).

Similarly, we illustrate the performance of the two-qubit scheme using the controlled Hadamard and controlled NOT gates as examples. According to the approximate conditions required to obtain the effective Hamiltonian $H'_{\text{eff}}$ in Eq. (13), we set $\Omega_3 = \Omega_4 = 2\pi \times 10$ MHz, $\Delta_3 = \Delta_4 = 10\Omega_4$, $U_{23} = U_{24} = U_{34} = 100\Delta_4$. As shown in Fig. 5, although there is a local phase between the subspaces $\{|10\rangle, |11\rangle\}$ and $\{|00\rangle, |01\rangle\}$ due to Stark shift, which makes the fidelity curve fluctuate significantly with time, the controlled Hadamard gate and NOT gate fidelities still reach 0.996 and 0.997, respectively, for the initial state $\psi(0) = \frac{1}{2}(|00\rangle + |01\rangle + |10\rangle + |11\rangle)$.

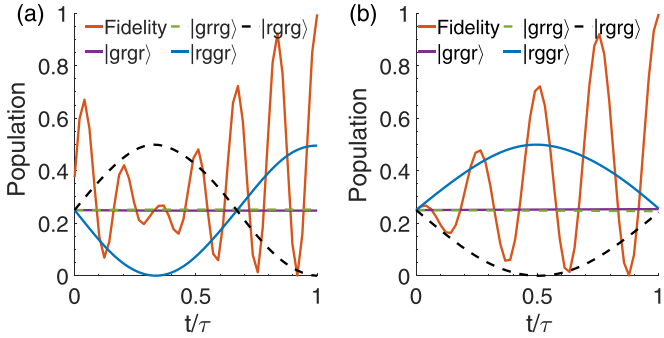


FIG. 5. Populations and fidelities of the constructed NNGQC-based two-qubit controlled Hadamard gate (a) and the constructed NNGQC-based two-qubit controlled NOT gate (b) with the initial state $\psi(0) = \frac{1}{2}(|00\rangle + |01\rangle + |10\rangle + |11\rangle)$.

Next, we demonstrate the robustness of two-qubit controlled gates based on our scheme to environmental errors. Using the two-qubit controlled Hadamard gate and two-qubit controlled NOT gates as examples, we compare our proposed NNGQC-based two-qubit controlled gate scheme with the NGQC-based two-qubit controlled gate scheme and DQC-based two-qubit controlled gate scheme under the influence of spontaneous emission and dephasing. As shown in Fig. 6, our scheme has certain advantages under the influence of decoherence error.

## IV. CONCLUSION

In conclusion, we have proposed an one-step implementation of NNGQC in DFS. A set of universal NNGQC-based single- and two-qubit gates is implemented in one step, which not only reduces the complexity and difficulty of the experimental operation but also reduces the impact of unavoidable environmental errors due to the short evolution time (NNGQC breaks the constraints of cyclic evolutionary conditions) and robustness to the collective decoherence of the system (DFS effectively prevents the collective decoherence).

## ACKNOWLEDGMENTS

This work was supported by the Special Project for Research and Development in Key Areas of Guangdong Province under Grant No. 2020B0303300001, the National Natural Science Foundation of China under Grants No. U21A20434, No. 12074346, No. 12147149, No. 12074390, and No. 91421111, and the Natural Science Foundation of Henan Province under Grant No. 212300410085.

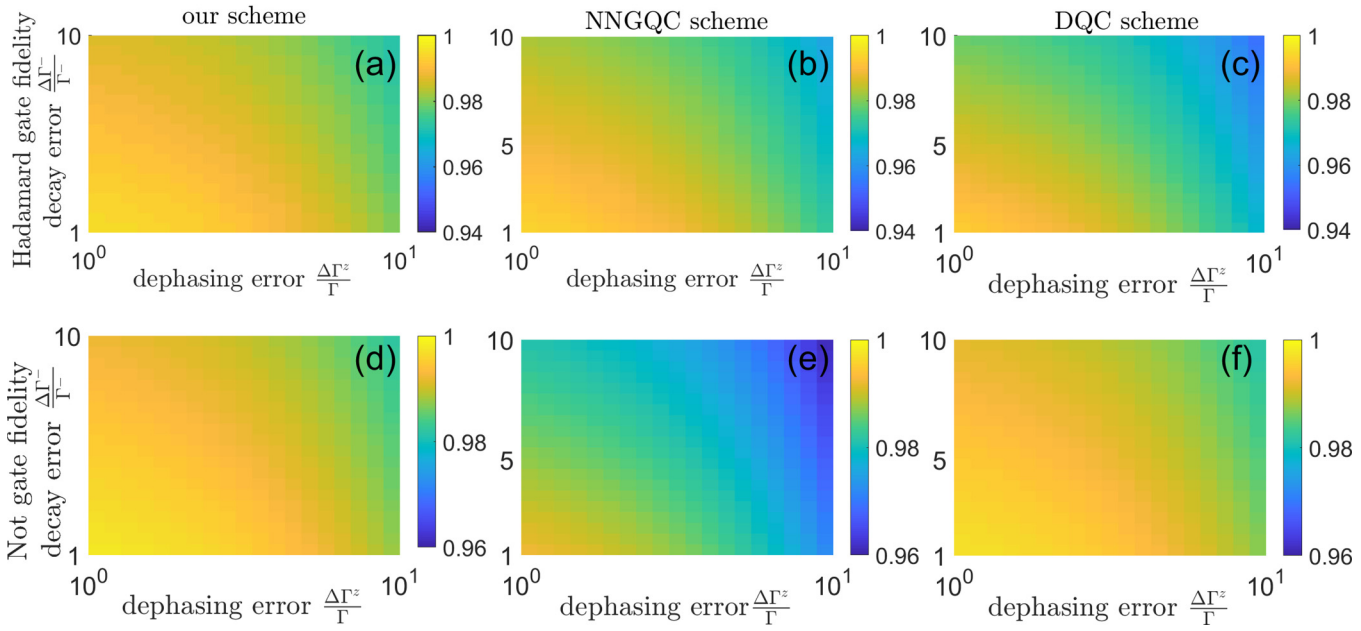


FIG. 6. The fidelities of the two-qubit controlled Hadamard gate in the case of NNGQC (a), NGQC (b), and DQC (c) and the two-qubit controlled NOT gate fidelity in the case of NNGQC (d), NGQC (e), and DQC (f) in DFS under spontaneous emission and dephasing, respectively.

## APPENDIX: DYNAMICAL SCHEME

Here we briefly describe the dynamical scheme mentioned above. Based on the effective Hamiltonian $H_{\text{eff}} = \Omega_{\text{eff}} e^{-i\varphi'}|0\rangle\langle 1| + \text{H.c.}$ in Eq. (4) we can obtain the evolution operator as

$$U(\Theta, \varphi') = \begin{pmatrix} \cos\Theta & -ie^{-i\varphi'}\sin\Theta \\ -ie^{i\varphi'}\sin\Theta & \cos\Theta \end{pmatrix}, \quad \text{(A1)}$$

where $\Theta = \Omega_{\text{eff}}\tau$ and $\tau$ is the laser operation time. When setting $\varphi' = \frac{3\pi}{2}$, we can obtain the quantum gate $U_y(\Theta) = e^{i\Theta\sigma_y}$, and when setting two sequential evolutions $U_1(\Theta = \frac{\pi}{2}, \varphi' = \frac{\varphi_z}{2})$ and $U_2(\Theta = \frac{\pi}{2}, \varphi' = \frac{-\varphi_z}{2})$ we can obtain the quantum gate $U_z(\varphi_z) = U_2U_1 = e^{i\varphi_z\sigma_z}$. $U_y(\Theta)$ and $U_z(\varphi_z)$ can be combined to form a universal set of quantum gates, i.e.,

$$\begin{aligned} U'(\Theta, \varphi_z) &= U_y(\Theta)U_z(\varphi_z) \\ &= U_y(\Theta)U_1U_2 \\ &= \begin{pmatrix} -e^{i\frac{\varphi_z}{2}}\cos\Theta & -e^{-i\frac{\varphi_z}{2}}\sin\Theta \\ e^{i\frac{\varphi_z}{2}}\sin\Theta & -e^{-i\frac{\varphi_z}{2}}\cos\Theta \end{pmatrix}. \end{aligned} \quad \text{(A2)}$$

For the NOT gate, its corresponding evolution operator is $U_{\text{NOT}} = U(\theta = \frac{\pi}{2}, \varphi' = \pi)$. In addition, the Hadamard gate is obtained in three steps; the parameters in Eq. (A2) are set as $U_H = U(\Theta = \frac{\pi}{4}, \varphi' = -\frac{3\pi}{2})U'(\Theta = \frac{\pi}{2}, \varphi' = -\frac{\pi}{2})U'(\Theta = \frac{\pi}{2}, \varphi' = \frac{\pi}{2})$.


[1] P. W. Shor, Polynomial-time algorithms for prime factorization and discrete logarithms on a quantum computer, SIAM J. Comput. **26**, 1484 (1997).

[2] L. K. Grover, Quantum Mechanics Helps in Searching for a Needle in a Haystack, Phys. Rev. Lett. **79**, 325 (1997).

[3] T. M. Graham, M. Kwon, B. Grinkemeyer, Z. Marra, X. Jiang, M. T. Lichtman, Y. Sun, M. Ebert, and M. Saffman, Rydberg-Mediated Entanglement in a Two-Dimensional Neutral Atom Qubit Array, Phys. Rev. Lett. **123**, 230501 (2019).

[4] D. Barredo, S. de Léséleuc, V. Lienhard, T. Lahaye, and A. Browaeys, An atom-by-atom assembler of defect-free arbitrary two-dimensional atomic arrays, Science **354**, 1021 (2016).

[5] S. Ebadi, T. T. Wang, H. Levine, A. Keesling, G. Semeghini, A. Omran, D. Bluvstein, R. Samajdar, H. Pichler, W. W. Ho, S. Choi, S. Sachdev, M. Greiner, V. Vuletić, and M. D. Lukin, Quantum phases of matter on a 256-atom programmable quantum simulator, Nature (London) **595**, 227 (2021).

[6] M. Endres, H. Bernien, A. Keesling, H. Levine, E. R. Anschuetz, A. Krajenbrink, C. Senko, V. Vuletic, M. Greiner, and M. D. Lukin, Atom-by-atom assembly of defect-free one-dimensional cold atom arrays, Science **354**, 1024 (2016).

[7] S. K. Mallavarapu, A. Niranjan, W. Li, S. Wüster, and R. Nath, Population trapping in a pair of periodically driven Rydberg atoms, Phys. Rev. A **103**, 023335 (2021).

[8] S. Basak, Y. Chougale, and R. Nath, Periodically Driven Array of Single Rydberg Atoms, Phys. Rev. Lett. **120**, 123204 (2018).

[9] D. Jaksch, J. I. Cirac, P. Zoller, S. L. Rolston, R. Côté, and M. D. Lukin, Fast Quantum Gates for Neutral Atoms, Phys. Rev. Lett. **85**, 2208 (2000).

[10] M. Saffman, T. G. Walker, and K. Mølmer, Quantum information with Rydberg atoms, Rev. Mod. Phys. **82**, 2313 (2010).

[11] W. Li and I. Lesanovsky, Entangling quantum gate in trapped ions via Rydberg blockade, Appl. Phys. B **114**, 37 (2014).

[12] S.-L. Su, F.-Q. Guo, L. Tian, X.-Y. Zhu, L.-L. Yan, E.-J. Liang, and M. Feng, Nondestructive Rydberg parity meter and its applications, Phys. Rev. A **101**, 012347 (2020).

[13] S.-L. Su and W. Li, Dipole-dipole-interaction–driven antiblockade of two Rydberg atoms, Phys. Rev. A **104**, 033716 (2021).

[14] J.-L. Wu, S.-L. Su, Y. Wang, J. Song, Y. Xia, and Y.-Y. Jiang, Effective Rabi dynamics of Rydberg atoms and robust high-fidelity quantum gates with a resonant amplitude-modulation field, Opt. Lett. **45**, 1200 (2020).

[15] L. Isenhower, E. Urban, X. L. Zhang, A. T. Gill, T. Henage, T. A. Johnson, T. G. Walker, and M. Saffman, Demonstration of a Neutral Atom Controlled-NOT Quantum Gate, Phys. Rev. Lett. **104**, 010503 (2010).

[16] H. Levine, A. Keesling, A. Omran, H. Bernien, S. Schwartz, A. S. Zibrov, M. Endres, M. Greiner, V. Vuletić, and M. D. Lukin, High-Fidelity Control and Entanglement of Rydberg-Atom Qubits, Phys. Rev. Lett. **121**, 123603 (2018).

[17] F. Wilczek and A. Zee, Appearance of Gauge Structure in Simple Dynamical Systems, Phys. Rev. Lett. **52**, 2111 (1984).

[18] M. V. Berry, Quantal phase factors accompanying adiabatic changes, Proc. R. Soc. A **392**, 45 (1984).

[19] Y. Aharonov and J. Anandan, Phase Change During a Cyclic Quantum Evolution, Phys. Rev. Lett. **58**, 1593 (1987).

[20] J. Pachos, P. Zanardi, and M. Rasetti, Non-Abelian Berry connections for quantum computation, Phys. Rev. A **61**, 010305(R) (1999).

[21] L.-M. Duan, J. I. Cirac, and P. Zoller, Geometric manipulation of trapped ions for quantum computation, Science **292**, 1695 (2001).

[22] L.-A. Wu, P. Zanardi, and D. A. Lidar, Holonomic Quantum Computation in Decoherence-Free Subspaces, Phys. Rev. Lett. **95**, 130501 (2005).

[23] Y.-Y. Huang, Y.-K. Wu, F. Wang, P.-Y. Hou, W.-B. Wang, W.-G. Zhang, W.-Q. Lian, Y.-Q. Liu, H.-Y. Wang, H.-Y. Zhang, L. He, X.-Y. Chang, Y. Xu, and L.-M. Duan, Experimental Realization of Robust Geometric Quantum Gates with Solid-State Spins, Phys. Rev. Lett. **122**, 010503 (2019).

[24] S.-L. Zhu and Z. D. Wang, Implementation of Universal Quantum Gates Based on Nonadiabatic Geometric Phases, Phys. Rev. Lett. **89**, 097902 (2002).

[25] P. Zhao, Z. Dong, Z. Zhang, G. Guo, D. Tong, and Y. Yin, Experimental realization of nonadiabatic geometric gates with a superconducting xmon qubit, Sci. China Phys. Mech. Astron. **64**, 250362 (2021).

[26] E. Sjöqvist, D. M. Tong, L. M. Andersson, B. Hessmo, M. Johansson, and K. Singh, Non-adiabatic holonomic quantum computation, New J. Phys. **14**, 103035 (2012).

[27] G. F. Xu, J. Zhang, D. M. Tong, E. Sjöqvist, and L. C. Kwek, Nonadiabatic Holonomic Quantum Computation in Decoherence-Free Subspaces, Phys. Rev. Lett. **109**, 170501 (2012).

[28] X.-K. Song, H. Zhang, Q. Ai, J. Qiu, and F.-G. Deng, Shortcuts to adiabatic holonomic quantum computation in decoherence-free subspace with transitionless quantum driving algorithm, New J. Phys. **18**, 023001 (2016).

[29] P. Z. Zhao, G. F. Xu, and D. M. Tong, Nonadiabatic holonomic multiqubit controlled gates, Phys. Rev. A **99**, 052309 (2019).

[30] M. Li, F.-Q. Guo, Z. Jin, L.-L. Yan, E.-J. Liang, and S.-L. Su, Multiple-qubit controlled unitary quantum gate for Rydberg atoms using shortcut to adiabaticity and optimized geometric quantum operations, Phys. Rev. A **103**, 062607 (2021).

[31] L.-N. Sun, L.-L. Yan, S.-L. Su, and Y. Jia, One-Step Implementation of Time-Optimal-Control Three-Qubit Nonadiabatic Holonomic Controlled Gates in Rydberg Atoms, Phys. Rev. Applied **16**, 064040 (2021).

[32] A. A. Abdumalikov Jr, J. M. Fink, K. Juliusson, M. Pechal, S. Berger, A. Wallraff, and S. Filipp, Experimental realization of non-abelian non-adiabatic geometric gates, Nature (London) **496**, 482 (2013).

[33] C. Song, S.-B. Zheng, P. Zhang, K. Xu, L. Zhang, Q. Guo, W. Liu, D. Xu, H. Deng, K. Huang, D. Zheng, X. Zhu, and H. Wang, Continuous-variable geometric phase and its manipulation for quantum computation in a superconducting circuit, Nat. Commun. **8**, 1061 (2017).

[34] S. Danilin, A. Vepsäläinen, and G. S. Paraoanu, Experimental state control by fast non-Abelian holonomic gates with a superconducting qutrit, Phys. Scr. **93**, 055101 (2018).

[35] Z. Zhang, P. Z. Zhao, T. Wang, L. Xiang, Z. Jia, P. Duan, D. M. Tong, Y. Yin, and G. Guo, Single-shot realization of nonadiabatic holonomic gates with a superconducting xmon qutrit, New J. Phys. **21**, 073024 (2019).

[36] Y. Xu, W. Cai, Y. Ma, X. Mu, L. Hu, T. Chen, H. Wang, Y. P. Song, Z.-Y. Xue, Z.-Q. Yin, and L. Sun, Single-Loop Realization of Arbitrary Nonadiabatic Holonomic Single-Qubit Quantum Gates in a Superconducting Circuit, Phys. Rev. Lett. **121**, 110501 (2018).

[37] C. Zu, W.-B. Wang, L. He, W.-G. Zhang, C.-Y. Dai, F. Wang, and L.-M. Duan, Experimental realization of universal geometric quantum gates with solid-state spins, Nature (London) **514**, 72 (2014).

[38] Y. Sekiguchi, N. Niikura, R. Kuroiwa, H. Kano, and H. Kosaka, Optical holonomic single quantum gates with a geometric spin under a zero field, Nat. Photon. **11**, 309 (2017).

[39] B. B. Zhou, P. C. Jerger, V. O. Shkolnikov, F. J. Heremans, G. Burkard, and D. D. Awschalom, Holonomic Quantum Control by Coherent Optical Excitation in Diamond, Phys. Rev. Lett. **119**, 140503 (2017).

[40] J. A. Jones, V. Vedral, A. Ekert, and G. Castagnoli, Geometric quantum computation using nuclear magnetic resonance, Nature (London) **403**, 869 (2000).

[41] Y. Ota, Y. Goto, Y. Kondo, and M. Nakahara, Geometric quantum gates in liquid-state NMR based on a cancellation of dynamical phases, Phys. Rev. A **80**, 052311 (2009).

[42] G. Feng, G. Xu, and G. Long, Experimental Realization of Nonadiabatic Holonomic Quantum Computation, Phys. Rev. Lett. **110**, 190501 (2013).

[43] H. Li, Y. Liu, and G. Long, Experimental realization of single-shot nonadiabatic holonomic gates in nuclear spins, Sci. China Phys. Mech. Astron. **60**, 080311 (2017).

[44] Z. Zhu, T. Chen, X. Yang, J. Bian, Z.-Y. Xue, and X. Peng, Single-Loop and Composite-Loop Realization of Nonadiabatic Holonomic Quantum Gates in a Decoherence-Free Subspace, Phys. Rev. Applied **12**, 024024 (2019).

[45] T. Chen, P. Shen, and Z.-Y. Xue, Robust and Fast Holonomic Quantum Gates with Encoding on Superconducting Circuits, Phys. Rev. Applied **14**, 034038 (2020).

[46] T. Chen and Z.-Y. Xue, High-Fidelity and Robust Geometric Quantum Gates that Outperform Dynamical Ones, Phys. Rev. Applied **14**, 064009 (2020).

[47] J. Xu, S. Li, T. Chen, and Z.-Y. Xue, Nonadiabatic geometric quantum computation with optimal control on superconducting circuits, Front. Phys. **15**, 41503 (2020).

[48] A. Friedenauer and E. Sjöqvist, Noncyclic geometric quantum computation, Phys. Rev. A **67**, 024303 (2003).

[49] B.-J. Liu, S.-L. Su, and M.-H. Yung, Nonadiabatic noncyclic geometric quantum computation in Rydberg atoms, Phys. Rev. Research **2**, 043130 (2020).

[50] J. W. Zhang, L.-L. Yan, J. C. Li, G. Y. Ding, J. T. Bu, L. Chen, S.-L. Su, F. Zhou, and M. Feng, Single-Atom Verification of the Noise-Resilient and Fast Characteristics of Universal Nonadiabatic Noncyclic Geometric Quantum Gates, Phys. Rev. Lett. **127**, 030502 (2021).

[51] D. A. Lidar, I. L. Chuang, and K. B. Whaley, Decoherence-Free Subspaces for Quantum Computation, Phys. Rev. Lett. **81**, 2594 (1998).

[52] L.-M. Duan and G.-C. Guo, Preserving Coherence in Quantum Computation by Pairing Quantum Bits, Phys. Rev. Lett. **79**, 1953 (1997).

[53] P. G. Kwiat, A. J. Berglund, J. B. Altepeter, and A. G. White, Experimental verification of decoherence-free subspaces, Science **290**, 498 (2000).

[54] M. Mohseni, J. S. Lundeen, K. J. Resch, and A. M. Steinberg, Experimental Application of Decoherence-Free Subspaces in an Optical Quantum-Computing Algorithm, Phys. Rev. Lett. **91**, 187903 (2003).

[55] D. Kielpinski, V. Meyer, M. A. Rowe, C. A. Sackett, W. M. Itano, C. Monroe, and D. J. Wineland, A decoherence-free quantum memory using trapped ions, Science **291**, 1013 (2001).

[56] G. Xu and G. Long, Universal nonadiabatic geometric gates in two-qubit decoherence-free subspaces, Sci. Rep. **4**, 6814 (2015).

[57] Z.-Y. Xue, J. Zhou, and Z. D. Wang, Universal holonomic quantum gates in decoherence-free subspace on superconducting circuits, Phys. Rev. A **92**, 022320 (2015).

[58] Z.-Y. Xue, J. Zhou, Y.-M. Chu, and Y. Hu, Nonadiabatic holonomic quantum computation with all-resonant control, Phys. Rev. A **94**, 022331 (2016).

[59] R. M. W. van Bijnen, Quantum engineering with ultracold atoms, Ph.D. thesis, Eindhoven University of Technology, Eindhoven, 2013; D. Cano and J. Fortágh, Multiatom entanglement in cold Rydberg mixtures, Phys. Rev. A **89**, 043413 (2014); Y.-M. Liu, X.-D. Tian, D. Yan, Y. Zhang, C.-L. Cui, and J.-H. Wu, Nonlinear modifications of photon correlations via controlled single and double Rydberg blockade, *ibid.* **91**, 043802 (2015).

[60] P. Xue and Y.-F. Xiao, Universal Quantum Computation in Decoherence-Free Subspace with Neutral Atoms, Phys. Rev. Lett. **97**, 140501 (2006).

[61] X.-L. Feng, C. Wu, H. Sun, and C. H. Oh, Geometric Entangling Gates in Decoherence-Free Subspaces with Minimal Requirements, Phys. Rev. Lett. **103**, 200501 (2009).

[62] B.-J. Liu, X.-K. Song, Z.-Y. Xue, X. Wang, and M.-H. Yung, Plug-and-Play Approach to Nonadiabatic Geometric Quantum Gates, Phys. Rev. Lett. **123**, 100501 (2019).

[63] J. Samuel and R. Bhandari, General Setting for Berry's Phase, Phys. Rev. Lett. **60**, 2339 (1988).

[64] Z. Zhou, Y. Margalit, S. Moukouri, Y. Meir, and R. Folman, An experimental test of the geodesic rule proposition for the noncyclic geometric phase, Sci. Adv. **6**, eaay8345 (2020).

[65] D. Manzano, A short introduction to the lindblad master equation, AIP Adv. **10**, 025106 (2020).

[66] I. I. Beterov, I. I. Ryabtsev, D. B. Tretyakov, and V. M. Entin, Quasiclassical calculations of blackbody-radiation-induced depopulation rates and effective lifetimes of Rydberg $ns$, $np$, and $nd$ alkali-metal atoms with $n \leqslant 80$, Phys. Rev. A **79**, 052504 (2009).

[67] X.-Y. Zhu, Z. Jin, E. Liang, S. Zhang, and S.-L. Su, Preparation of steady 3d dark state entanglement in dissipative Rydberg atoms via electromagnetic induced transparency, Ann. der Phys. **532**, 2000059 (2020).

[68] P. Z. Zhao, X.-D. Cui, G. F. Xu, E. Sjöqvist, and D. M. Tong, Rydberg-atom-based scheme of nonadiabatic geometric quantum computation, Phys. Rev. A **96**, 052316 (2017).

[69] S.-B. Zheng, C.-P. Yang, and F. Nori, Comparison of the sensitivity to systematic errors between nonadiabatic non-Abelian geometric gates and their dynamical counterparts, Phys. Rev. A **93**, 032313 (2016).